Long-range four-body interactions in structured nonlinear photonic waveguides

Xin Wang [1,2] Jia-Qi Li [1] Tao Liu,[3,*] Adam Miranowicz [4,2] and Franco Nori[2,5]

[1]*Institute of Theoretical Physics, School of Physics, Xi'an Jiaotong University, Xi'an 710049, People's Republic of China*

[2]*Quantum Computing Center, RIKEN, Wakoshi, Saitama 351-0198, Japan*

[3]*School of Physics and Optoelectronics, South China University of Technology, Guangzhou 510640, China*

[4]*Institute of Spintronics and Quantum Information, Faculty of Physics, Adam Mickiewicz University, 61-614 Poznań, Poland*

[5]*Physics Department, The University of Michigan, Ann Arbor, Michigan 48109-1040, USA*

(Received 8 January 2024; revised 12 August 2024; accepted 12 November 2024; published 2 December 2024)

Multiphoton dynamics beyond linear optical materials are of significant fundamental and technological importance in quantum information processing. However, it remains largely unexplored in nonlinear waveguide QED. In this work, we theoretically propose a structured nonlinear waveguide in the presence of staggered photon-photon interactions, which supports two branches of gaped bands for doublons (i.e., spatially bound-photon-pair states). In contrast to linear waveguide QED systems, we identify two important contributions to its dynamical evolution, i.e., single-photon bound states (SPBSs) and doublon bound states (DBSs). Most remarkably, the nonlinear waveguide can mediate the long-range four-body interactions between two emitter pairs, even in the presence of disturbance from SPBSs. By appropriately designing system's parameters, we can achieve high-fidelity four-body Rabi oscillations mediated only by virtual doublons in DBSs. Our findings pave the way for applying structured nonlinear waveguide QED in multi-body quantum information processing and quantum simulations among remote sites.

DOI: 10.1103/PhysRevResearch.6.043226

I. INTRODUCTION

The past few years have witnessed a surge of interest in the field of waveguide quantum electrodynamics (QED) in structured linear optical materials without photon-photon interactions, leading to intriguing phenomena such as unconventional bound states, non-Markovian evolution and chiral emissions [1–15]. In these linear optical waveguides, dynamical properties are governed and investigated at the single-photon level [16–23]. However, once quantum many-body interactions between individual .photons are introduced, standard descriptions based on single-photon properties are inadequate [24–36]. These nonlinear quantum optics phenomena can find important applications in fields of quantum information and metrology [32,37–41].

In artificial platforms, such as nanophotonic structures and circuit-QED, strong nonlinear interactions can be experimentally realized [42–47], providing ideal platforms for exploring quantum effects at the level of few photons and effects of many-body statistics on waveguide QED [48–61]. Recently, a remarkable supercorrelated radiance phenomenon, beyond the conventional super- and subradiance, was reported in a nonlinear waveguide QED system with nonstructured bath [62]. Until now, in spite of potentiallyinteresting physics hidden behind it, the field of nonlinear waveguide QED remains largely unexplored. Along previous works in this field [62–65], a natural question arises: How does the structured nonlinear waveguide QED system influence the dynamics in the presence of a strong photon-photon interaction.

Here we consider emitter pairs interacting with a structured nonlinear waveguide by designing a staggered onsite photon-photon interaction. In contrast to previous work [62–65], we find the formation of gaped bands for doublons, i.e., spatially bound-photon-pair states [66–79]. We reveal the effects of both doublon bound states (DBSs) and single-photon bound states (SPBSs) on the evolution dynamics of the hybrid system. Most remarkably, we demonstrate *long-range four-body interactions*, mediated by DBSs, between distant emitter pairs. We find that a high-fidelity four-body interaction requires two emitter pairs for a separation larger than the size of the SPBS to prevent undesired single-photon-mediated transitions. Our study shows a remarkable different physics in the nonlinear waveguide QED regime in contrast with conventional linear systems.

II. DOUBLON ENERGY BANDS

We consider a nonlinear waveguide constructed by an array of coupled cavities in the presence of strong photon-photon interactions (see Fig. 1). In the rotating frame of the cavity frequency, the Hamiltonian of the waveguide is written as

$$H_w = -J\sum_n (a_n^\dagger a_{n+1} + \text{H.c.}) - \frac{1}{2}\sum_n U_n a_n^\dagger a_n^\dagger a_n a_n, \quad (1)$$

where J is the bosonic hopping strength, U_n denotes the Kerr nonlinearity at site n, and $a_n^\dagger$ is the annihilation operator of nth cavity. To realize a structured environment, we introduce the staggered photon-photon interaction with

*Contact author: liutao0716@scut.edu.cn

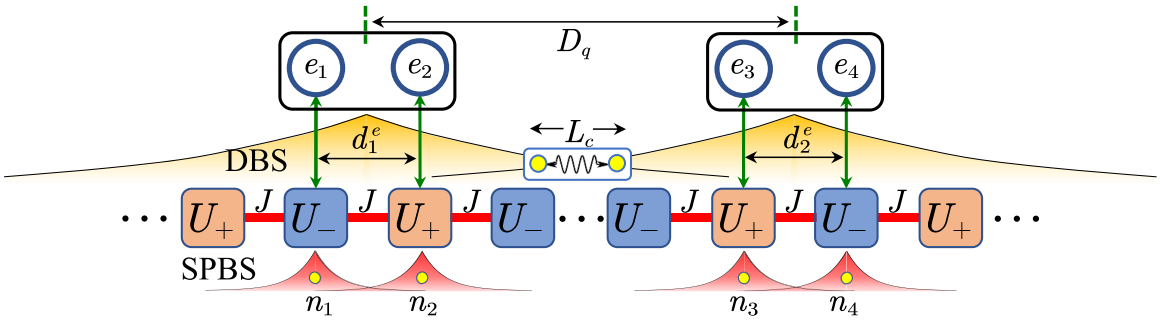

FIG. 1. Schematic of the nonlinear QED setup, with a waveguide consisting of coupled cavity arrays in the presence of a Kerr nonlinearity. Here J is the photonic hopping strength, and $U_\pm = U_c \pm U_m$ denotes the staggered onsite photon-photon interaction. The emitter pair $e_{1,2}$ is separated from the pair $e_{3,4}$ by a distance D_q, while d_1^e and d_2^e are the distance of each emitter pair. In the dynamical evolution, a doublon bound state (DBS), corresponding to a virtual exchange process of two photons with correlated length L_c, is considered, accompanied by single-photon bound state (SPBSs) due to the virtual exchange of a single photon.

$U_n = U_c + (-1)^n U_m$ (where $U_c \pm U_m$ is the staggered interaction strength). We numerically calculate the two-photon spectrum as a function of U_c for $N = 100$ with periodic boundary condition (by setting $J = 1$), as shown in Fig. 2(a).

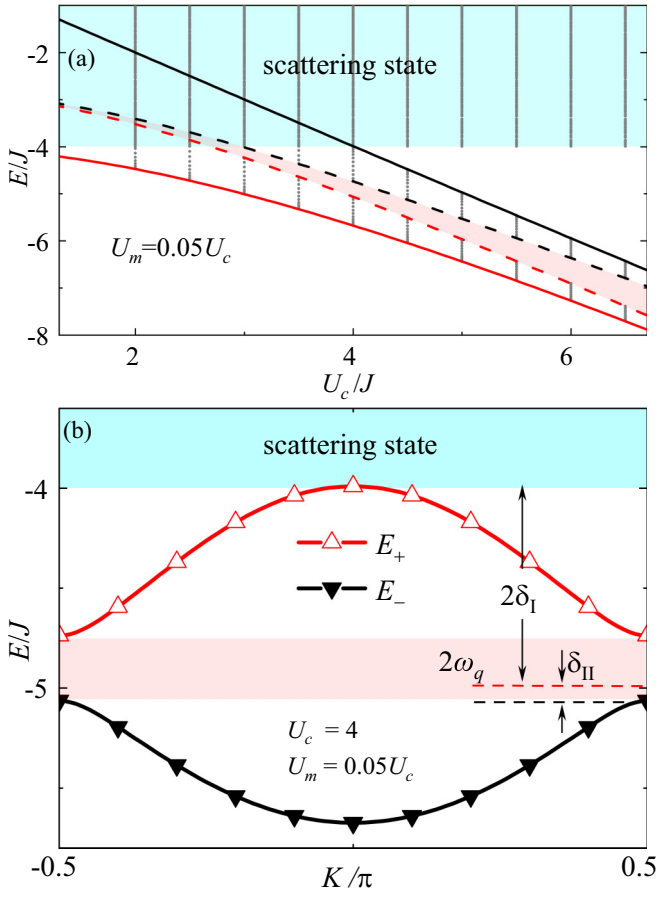

FIG. 2. (a) Two-excitation spectrum of the Hamiltonian H_w versus the mean value U_c. The curves represent the upper and lower bounds of the doublon energy bands in Eq. (23). (b) Doublon's spectrum for $U_c = 4J$ and $U_m = 0.05U_c$. The emitter-pair frequency $2\omega_q$ lies inside the doublon band gap with a detuning δ_{II} ($2\delta_I$) to the lower band (scattering states). The cyan (pink) region corresponds to the scattering states (doublon band gap).

Besides continuum scattering states, there exist discrete doublon energy bands with bound photon pairs. In addition, the doublon bands become distinctly separated from the scattering states for $U_c > 4J$.

The doublon spectrum can be analytically solved by defining the center-of-mass and relative coordinates, i.e., $x_c = (m+n)/2$ and $r = m - n$, with m and n representing the positions of the two photons. Given that the Hilbert space is confined to a two-photon subspace, the nonlinear term can be expressed as

$$H_U = V(x_c, r) = [U_c + U_m \cos(\pi x_c)]\delta_{r0}, \tag{2}$$

where δ_{r0} is a delta function that is nonzero solely when $r = 0$ and x_c is restricted to be integers. It is important to mention that H_U is modulated periodically in the x_c direction. Applying the Bloch theorem, the eigen wave function of the doublon can be written as

$$\Psi(m, n) = \frac{1}{\sqrt{N}} \exp(iKx_c) u_K(x_c, r), \tag{3}$$

where $u_K(x_c, r)$ is a periodic function satisfying $u_K(x_c, r) = u_K(x_c + 2, r)$. In our study, the nonlinearity varies between nearest-neighbor sites, which results in the Fourier series having only two terms in the x_c direction. We utilize a wave-function ansatz in a separable variable form,

$$u_K(x_c, r) = \psi_K^{(0)}(r) + e^{i\pi x_c} \psi_K^{(1)}(r). \tag{4}$$

The dispersion relation and wave functions are derived by solving the Schrödinger equation

$$[H_0 + \delta_{r0} H_U] \begin{bmatrix} \psi_K^{(0)} \\ \psi_K^{(1)} \end{bmatrix} = E \begin{bmatrix} \psi_K^{(0)} \\ \psi_K^{(1)} \end{bmatrix}. \tag{5}$$

First, we start from the nonperturbation part, ignoring H_U. The first term in Eq. (4) is

$$H_0 e^{iK\frac{m+n}{2}} \psi_K^{(0)}(m-n) = -J \sum_{\pm} \Big[e^{iK\frac{m\pm1+n}{2}} \psi_K^{(0)}(m \pm 1 - n) + e^{iK\frac{m+n\pm1}{2}} \psi_K^{(0)}(m - n \mp 1) \Big], \tag{6}$$

which can be simplified as

$$H_0\psi_K^{(0)}(r) = -2J\cos\left(\frac{K}{2}\right)\sum_{\pm}\psi_K^{(0)}(r\pm 1). \tag{7}$$

Similarly, the second term in Eq. (4) is

$$H_0\psi_K^{(1)}(r) = -2J\cos\left(\frac{K+\pi}{2}\right)\sum_{\pm}\psi_K^{(1)}(r\pm 1). \tag{8}$$

Then H_0 is rewritten as

$$\begin{aligned} H_0 &= \begin{vmatrix} H_{00} & H_{10} \\ H_{01} & H_{11} \end{vmatrix} \\ &= \begin{vmatrix} -2J\cos\left(\frac{K}{2}\right)\Delta^\dagger(r) & 0 \\ 0 & -2J\cos\left(\frac{K+\pi}{2}\right)\Delta^\dagger(r) \end{vmatrix}, \end{aligned} \tag{9}$$

with

$$\Delta^\dagger(r)\psi_K^i(r) = \left[\psi_K^{(i)}(r+1) + \psi_K^{(i)}(r-1)\right].$$

The photon-photon interaction term H_U is written as

$$H_U = \begin{vmatrix} U_{00} & U_{10} \\ U_{01} & U_{01} \end{vmatrix}, \tag{10}$$

where the matrix elements are respectively derived as:

$$U_{00} = \frac{1}{N}\sum_{x_c\in\mathbb{Z}} e^{-iKx_c}H_U e^{iKx_c} = U_c, \tag{11}$$

$$U_{01} = U_{10}^* = \frac{1}{N}\sum_{x_c\in\mathbb{Z}} e^{-iKx_c}H_U e^{iKx_c}e^{i\pi x_c} = U_m, \tag{12}$$

$$U_{11} = \frac{1}{N}\sum_{x_c\in\mathbb{Z}} e^{-iKx_c}e^{-i\pi x_c}H_U e^{iKx_c}e^{i\pi x_c} = U_c, \tag{13}$$

where $H_U = U_c + U_m\cos(\pi x_c)$. By defining the Green function as

$$(E - H_0)G_K(E, r) = \delta_{r0}, \tag{14}$$

we obtain the Lippmann-Schwinger equation for the doublon states

$$\begin{aligned} \Psi_K(r) &= \Psi_0(r) + \int G_K(E, r-r')\,\delta_{r0}\,H_U\,\Psi(r')\,dr', \\ \Psi_K(r) &= \begin{bmatrix} \psi_K^{(0)}(r) \\ \psi_K^{(1)}(r) \end{bmatrix}, \end{aligned} \tag{15}$$

where $\Psi_0(r)$ is the solution satisfying the noninteracting Hamiltonian H_0. Employing the properties of the δ function, we obtain

$$\Psi_K(r) = \Psi_0(r) + G_K(E, r)H_U\Psi_K(r=0). \tag{16}$$

Finally, the wave function at $r = 0$ is derived as

$$[1 - G_K(E, r=0)H_U]\Psi_K(r=0) = \Psi_0(r=0). \tag{17}$$

The probability of the scattering state, where the two photons are not bound together, is zero; which corresponds to $\Psi_0(r) \equiv 0$. Consequently, the doublon state corresponds to the nontrivial solution of the linear homogeneous equations in Eq. (17),

$$\det\left[1 - G_K(E, r=0)H_U\right] = 0, \tag{18}$$

from which the dispersive relation of the doublon spectrum is obtained. The Green function in momentum space reads

$$G_K(E, r) = \frac{1}{2\pi}\int_{-\pi}^{\pi} dq\; G_K(E, q)\; e^{iqr}. \tag{19}$$

By substituting Eq. (19) into Eq. (14) and employing the properties of the δ function, we obtain

$$\begin{aligned} G_K(E, q) &= \frac{1}{(E - H_0)} \\ &= \begin{vmatrix} \frac{1}{E+4J\cos\left(\frac{K}{2}\right)\cos q} & 0 \\ 0 & \frac{1}{E-4J\sin\left(\frac{K}{2}\right)\cos q} \end{vmatrix}. \end{aligned} \tag{20}$$

Consequently, the Green function in real space is derived as

$$\begin{aligned} G_K(E, r) &= \begin{vmatrix} f_K^{(0)}(E, r) & 0 \\ 0 & f_K^{(1)}(E, r) \end{vmatrix}, \\ f_K^{(0)}(E, r) &= \int_{-\pi}^{\pi} \frac{e^{iqr}}{E + 4J\cos\left(\frac{K}{2}\right)\cos q}dq, \\ f_K^{(1)}(E, r) &= \int_{-\pi}^{\pi} \frac{e^{iqr}}{E - 4J\sin\left(\frac{K}{2}\right)\cos q}dq. \end{aligned} \tag{21}$$

By setting $r = 0$, we write Eq. (17) as

$$1 - G_K(E, r=0)H_U = \begin{vmatrix} \frac{U_c}{U_{\cos}} - 1 & \frac{U_m}{U_{\cos}} \\ \frac{U_m}{U_{\sin}} & \frac{U_c}{U_{\sin}} - 1 \end{vmatrix}, \tag{22}$$

where

$$\begin{aligned} U_{\cos} &= \sqrt{E^2 - 16[J\cos(K/2)]^2}, \\ U_{\sin} &= \sqrt{E^2 - 16[J\sin(K/2)]^2}. \end{aligned}$$

Altogether, the eigenenergy E and the momentum of center-of-mass K satisfy the following relationship:

$$\det\begin{vmatrix} \frac{U_c}{U_{\cos}} - 1 & \frac{U_m}{U_{\cos}} \\ \frac{U_m}{U_{\sin}} & \frac{U_c}{U_{\sin}} - 1 \end{vmatrix} = 0. \tag{23}$$

We plot two branches of the doublon bands in Fig. 2(b) according to Eq. (23), where a band gap exists.

Moreover, the amplitudes $\psi_K^{(1,2)}(r=0)$ correspond to the nontrivial solution of the linear homogeneous equations in Eq. (17). Therefore

$$\begin{aligned} &[1 - G_K(E, r=0)H_U]\begin{bmatrix} \psi_K^{(0)}(r=0) \\ \psi_K^{(1)}(r=0) \end{bmatrix} = \begin{bmatrix} 0 \\ 0 \end{bmatrix} \\ &\longrightarrow \frac{\psi_K^{(0)}(r=0)}{\psi_K^{(1)}(r=0)} = \frac{U_m U_{\sin}}{U_{\sin}U_{\cos} - U_c U_{\cos}}. \end{aligned} \tag{24}$$

By substituting Eq. (24) into Eq. (16), we derive the wave functions for the doublon eigenstates as

$$\Psi(r) = \begin{bmatrix} \psi_K^{(0)}(r) \\ \psi_K^{(1)}(r) \end{bmatrix} = G(E,r)H_U \begin{bmatrix} \psi_K^{(0)}(r=0) \\ \psi_K^{(1)}(r=0) \end{bmatrix} = \begin{vmatrix} f_K^{(0)}(E,r) & 0 \\ 0 & f_K^{(1)}(E,r) \end{vmatrix} \begin{vmatrix} U_c & U_m \\ U_m & U_c \end{vmatrix} \begin{bmatrix} \psi_K^{(0)}(r=0) \\ \psi_K^{(1)}(r=0) \end{bmatrix}, \tag{25}$$

where we have employed the condition $\Psi_0(r) \equiv 0$. Via analysis the integral Eq. (21), we obtain the formal solution of the wave function

$$\Psi_K(x_c, r) \propto \exp\left[-\frac{|r|}{L_c(K)}\right], \tag{26}$$

which $L_c(K)$ is the correlated length of the photon pair. In particular, at the band edge with zero group velocity, the wave functions $\Psi_K^{\pm}$ at $K_0 = \pi/2$ of the upper and lower bands can be analytically obtained as (see Appendix A)

$$\Psi_{K_0}^{\mp}(x_c, r) = \frac{e^{iK_0 x_c}(1 \pm e^{i\pi x_c})}{\sqrt{N}\psi_0} \exp\left[-\frac{|r|}{L_c^{\mp}(K_0)}\right], \tag{27}$$

where ψ_0 is the normalization factor, and the correlated length is

$$L_c^{\mp}(K_0) = \left(\ln \frac{2\sqrt{2}J}{-E_{\mp} - \sqrt{E_{\mp}^2 - 8J^2}}\right)^{-1}.$$

A strong on-site nonlinear interaction results in supercorrelated doublon modes. According to Eq. (27), $L_c^{\mp}(K_0) \sim 1$ for $U_c \simeq 4J$, indicating that the two photons are strongly bunched in space.

III. DYNAMICS AND BOUND STATES

A. Dynamics evolution

We consider two emitters e_1 and e_2, which are separated by a distance d_1^e, interacting with the nonlinear waveguide at points n_1 and n_2 (see Fig. 1). The hybrid system's Hamiltonian is

$$H = H_w + \frac{\omega_q}{2}\sum_{i=1}^{2}\sigma_i^z + g\sum_{i=1}^{2}(\sigma_i^+ a_{n_i} + \text{H.c.}), \tag{28}$$

where $a_{n_i}^{\dagger}$ is the annihilation operator of the bosonic mode interacting with the ith emitter, ω_q is the emitter frequency, and g is the coupling strength between each emitter and the waveguide. When the two-emitter excitation frequency $2\omega_q$ is set in the band gap between the doublon bands [see Fig. 2(b)], the evolution becomes highly non-Markovian owing to the van Hove singularity in the density of states [3], which is different from the case of unstructured nonlinear waveguides [62].

We now proceed to calculate the dynamics in the double-excitation subspace. We assume two emitters initially in their excited states, and their frequencies are chosen to be close to the lower band edge, with frequency detuning $\delta_{II} = 2\omega_q - E_-(K_0) \simeq 0$ [see Fig. 2(b)]. Since H in Eq. (28) conserves the excitation number, in the double-excitation subspace, the state $|\psi_2(t)\rangle$ is

$$|\psi_2(t)\rangle = c_e(t)|ee, \text{vac}\rangle + \sum_K c_K(t)|gg, \Psi_K^-\rangle + \sum_k [c_{1k}(t)|eg\rangle + c_{2k}(t)|ge\rangle]a_k^{\dagger}|\text{vac}\rangle, \tag{29}$$

where $c_e(t)$ $[c_K(t)]$ is the probability amplitude for two emitters (doublon states $|\Psi_K^-\rangle$) being excited, $a_k^{\dagger} = \sum_n e^{ikn}a_n^{\dagger}/\sqrt{N}$ is the single-photon creation operator in momentum space, and c_{ik} is the probability amplitude for the emitter i and the mode k being simultaneously excited. Because ω_q is significantly detuned from the scattering states (i.e., $\delta_I = |\omega_q - 2J| \gg g$), we have neglected their contributions in Eq. (29), and the one-photon state can also be adiabatically eliminated. Hence, we obtain the evolution equation (more detain in Appendix B 1)

$$i\dot{c}_e(t) = -\frac{1}{\sqrt{N}}\sum_K \mathcal{G}_K(n_1, n_2)c_K(t), \tag{30}$$

$$i\dot{c}_K(t) = \Delta_K c_K - \frac{1}{\sqrt{N}}\mathcal{G}_K^*(n_1, n_2)c_e(t), \tag{31}$$

where the emitter pair couples to the doublon mode K with an effective transition rate

$$\mathcal{G}_K(n_1, n_2) = g^2 \sum_{i,j=1,2}^{i\neq j}\sum_k \frac{e^{ikn_j}}{\delta_k} M(K, k, n_i), \tag{32}$$

where $M(K, k, n_i) = \langle k, n_i|\Psi_K^-\rangle$ denotes the process which annihilating one photon at position n_i and another photon with mode k to create a doublon mode K. Hence, we can simplify Eq. (32) as

$$\mathcal{G}_K(n_1, n_2) \propto \sum_{i,j=1,2}^{i\neq j}\sum_n \Psi_K^-\left(\frac{n+n_j}{2}, n_j - n\right)\psi_i(n), \tag{33}$$

which is proportional to the overlap between the doublon mode Ψ_K^- and a SPBS $\psi_i(n)$. This quantity implies the following dual processes: the emitter $i(j)$ excites a SPBS, distributing in the waveguide around the site $n_i(n_j)$; meanwhile, the emitter $j(i)$ excites another photon at $n_j(n_i)$. The overlap between this two photon pairs and the doublon state Ψ_K^- will excite the doublon mode K. As discussed in Appendix B 2, the formula of SPBS is

$$\psi_i(n) \simeq A_s \exp\left(-\frac{|n - n_i|}{L_I^B}\right), \quad \frac{1}{L_I^B} = \ln\frac{2J}{|\omega_q| - \sqrt{\omega_q^2 - 4J^2}}, \quad A_s = \frac{gJ}{\sqrt{\omega_q^2 - 4J^2}}, \tag{34}$$

where L_I^B (A_s) is the decay length (amplitude) of the SPBS. Note that $\mathcal{G}_K$ can be simplified further as

$$\mathcal{G}_K(n_i, n_j) \propto \sum_n \exp\left[-\frac{|n - n_j|}{L_c^-(K)}\right]\exp\left(-\frac{|n - n_i|}{L_I^B}\right), \tag{35}$$

which is decided by the decay length of double mode and SPBS, i.e., $\{L_c^-(K), L_I^B\}$ [62]. If $|n_i - n_j| \gg \max\{L_c^-(K), L_I^B\}$, then $\mathcal{G}_K(n_1, n_2)$ decreases to zero, which implies the emitter pair decouples to the doublon mode.

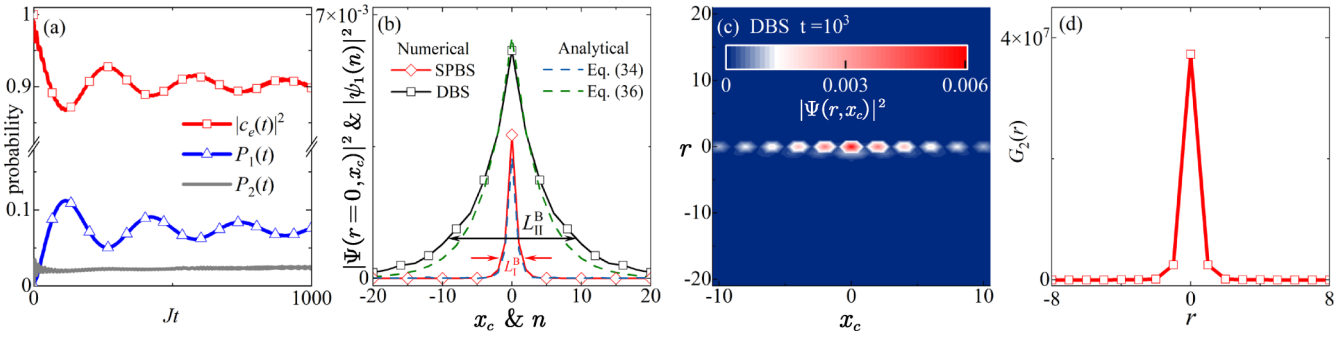

FIG. 3. (a) Time-dependent probability of the two-emitter excitations $|c_e(t)|^2$, and single- and two-photon excitations $P_{1,2}(t)$ for initially two-emitter excitation. The coupling points are set at $n_{1,2} = 0$. (b) The squared modulus of wave-function profile of the SPBS and DBS (by restricting $r = 0$) obtained via numerical simulations up to $t = 10^3$. (c) Two-dimensional field distribution for the DBS. (d) Two-point correlation function $G_2(r)$ for the field in (c). Here we set $J = 1$, $g = 0.1$, $U_c = 4$, $U_m = 0.05U_c$, $\alpha \simeq 2$, and $\delta_{II} = 0.03$.

B. Doublon bound state

As shown in Fig. 2 the pink region, due to the nonlinear periodic structure $U_n = U_c + (-1)^n U_m$, energy gap emerges in the band. Basis on this band gap, we realize DBSs, a new bound states which contains two supercorrelated photons. By setting the two-emitter excitation frequency $2\omega_q$ lies inside the doublon, the emitter pair is prevented from radiating doublons. Part of their excitation is trapped in the form of DBS. In Fig. 3(a), we plot the dynamic evolution in a finite-size waveguide with $N = 1000$, which is long enough to avoid the field being reflected by the open boundaries of the waveguide. By approximating the dispersion relation around $E_-(K_0)$ as a quadratic form with curvature α, i.e., $\Delta_K \simeq \delta_{II} + \alpha(K - K_0)^2$, the analytical wave function of the DBS is derived as (more detail in Appendix B 3)

$$\Psi_d(x_c, r) \simeq A_d(1 + e^{i\pi x_c}) \exp\left(-\frac{r}{L_c}\right) \exp\left(-\frac{|x_c - x_m|}{L_{II}^B}\right),$$
$$A_d = \frac{\mathcal{G}^*_{K_0}(n_1, n_2)}{\psi_0\sqrt{\delta_{II}\alpha}}, \quad L_{II}^B = \sqrt{\frac{\alpha}{\delta_{II}}}, \tag{36}$$

where $x_m = n_1 + n_2$. It shows that the decay length L_{II}^B of the DBS is determined by the detuning δ_{II} and the band curvature. Given the proximity of $2\omega_q$ to the band edge, the stationary DBS can extend a considerable distance from the coupling points. Because only the modes around K_0 are excited with high probabilities, the correlation length is approximated as $L_c^-(K_0)$. Note that, due to the DBSs, a new decay length L_{II}^B emerges in the x_c direction.

In Figs. 3(b) and 3(c), we plot the squared modulus of long-time field distribution for single- and two-photon states, corresponding to SPBS and DBS described in Eqs. (34) and (36). Owing to L_I^B and L_{II}^B is inversely proportional to δ_I and δ_{II}, respectively. Hence, under the setup of Fig. 2, both the amplitude and decay length of the DBS can be considerably larger than for the SPBS, i.e., $A_d > A_s$ and $L_{II}^B \gg L_I^B$. This is also manifested in Fig. 3(a), where the single-photon probability $P_1 = \sum_{i,k} |c_{ik}(t)|^2$, which is obtained numerically, is much lower than the two-photon probability $P_2 = \sum_K |c_K(t)|^2$ after a long-time evolution. In the DBS, the two virtual photon are strongly bound with a correlation length $L_c^-(K_0) \simeq 1$, as shown in the r direction of Fig. 3(c). To quantify this scale, we introduce the two-point correlation function for the DBS

$$G_2(r) = \sum_n \frac{\langle a_n^\dagger a_{n+r}^\dagger a_{n+r} a_n\rangle}{\langle a_{n+r}^\dagger a_{n+r}\rangle\langle a_n^\dagger a_n\rangle}. \tag{37}$$

As shown in Fig. 3(d), the decay length of $G_2(r)$ is of the same order as $L_c^-(K_0) \simeq 1$, and the two photons are strongly bunched in space. Therefore, we realize two photons bound state with supercorrelated photon pair, which two photons can't be separated and are jointly located around the coupling points.

IV. FOUR-BODY INTERACTIONS

Via the nonlinear potential, the waveguide can mediate four-body interactions. To demonstrate this, we consider two emitter pairs coupled to the common nonlinear waveguide, as depicted in Fig. 1. The separation distance between the center of each pair is set as D_q. In the nonlinear waveguide, there are two kinds of virtual processes due to the wave-function overlaps of DBSs for two emitter pairs and SPBSs for emitters

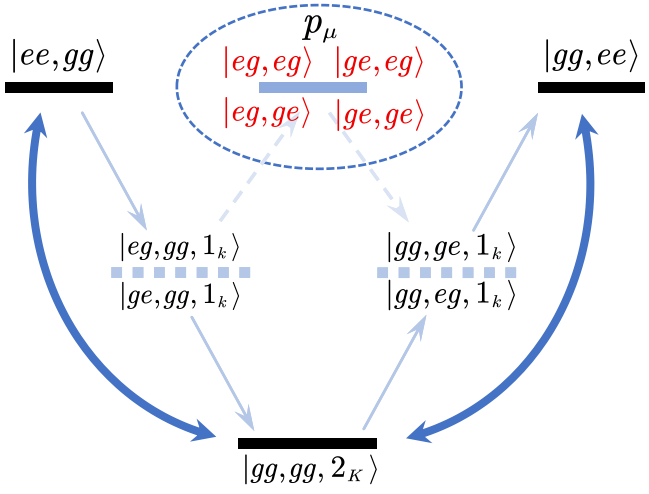

FIG. 4. Illustration of the transitions mediated by the SPBSs and DBSs, respectively. To enhance the fidelity of four-body Rabi oscillations, the unwanted single-photon transition processes (dash lines) should be suppressed.

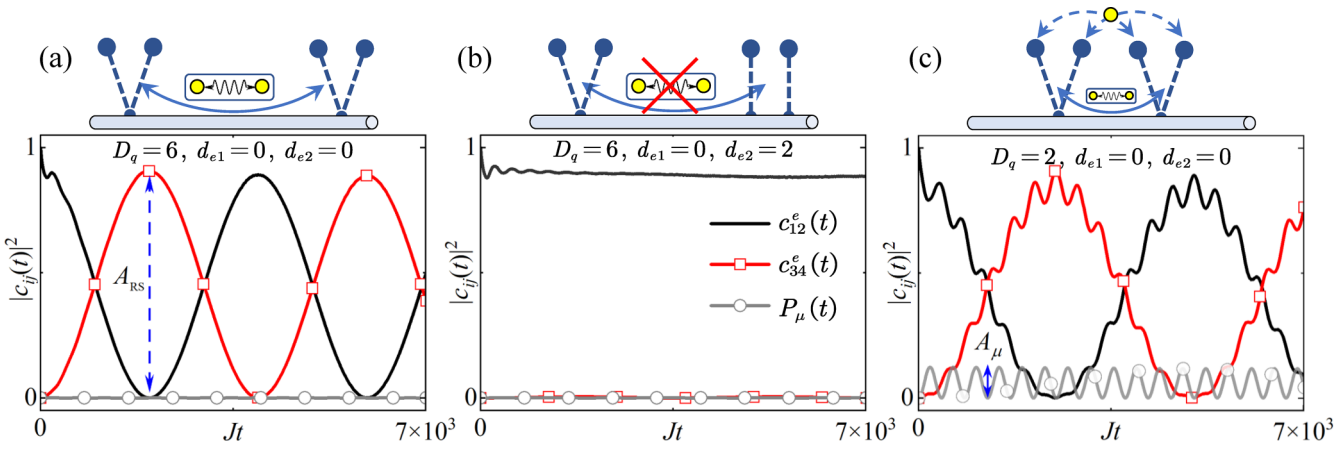

FIG. 5. [(a)–(c)] Four-body Rabi oscillations between two emitter pairs under different distance conditions. The amplitude of the four-body Rabi oscillation (single-photon transitions) is denoted as $A_{\rm RS}$ (A_μ). Same parameters as in Fig. 3.

in different pairs. For the former case, the virtual exchange between two-doublon states leads to a *four-body interaction* associated with the transition $|ee, gg\rangle \leftrightarrow |gg, ee\rangle$, as shown in Fig. 4. The four-body transition is a band-gap interaction which can avoid dissipations led by the doublon continuous modes.

For the latter case, the virtual exchange of a single photon induced a conventional two-body interaction. For instance, as shown in Fig. 4, the overlap between two SPBSs of emitters 1 and 3 cause a two-body interaction associated with the transition $|ee, gg\rangle$ and $|ge, eg\rangle$. There exist four distinct single-photon transition paths (see Fig. 4), and the total oscillating amplitude is $P_\mu = \sum_{ij\neq 12,34} |c^e_{ij}(t)|^2$, where $c^e_{ij}(t)$ denotes the probability for emitters, labeled by i, j, in the excited states.

For realizing high-fidelity four-body Rabi oscillations, the distance D_q is set as $\gg L^B_I$, which prevents any overlap between the SPBSs of emitters in different pairs and suppress the single-photon transition. Under the appropriate parameters, $P_\mu \simeq 0$, as shown in Fig. 5(a). With $P_\mu \simeq 0$, the system can be described by an effective four-body interaction Hamiltonian

$$H_{\rm RS} = \Delta_{S1}\sigma_1^+\sigma_2^+\sigma_1^-\sigma_2^- + \Delta_{S2}\sigma_3^+\sigma_4^+\sigma_3^-\sigma_4^- + (J_{\rm RS}\sigma_1^-\sigma_2^-\sigma_3^+\sigma_4^+ + \text{H.c.}), \tag{38}$$

where

$$\Delta_{Si} = \frac{1}{N}\sum_K \frac{|\mathcal{G}_{iK}|^2}{\Delta_K}, \quad J_{\rm RS} = -\frac{1}{\pi}\int_0^\pi \frac{\mathcal{G}_{1K}\mathcal{G}^*_{2K}}{\Delta_K}dK, \tag{39}$$

$$\mathcal{G}_{1K} = \mathcal{G}_K(n_1, n_2), \quad \mathcal{G}_{2K} = \mathcal{G}_K(n_3, n_4). \tag{40}$$

The first two term in Eqs. (38) correspond to dynamical Stark shifts, and $\Delta_{S1} = \Delta_{S2}$ given that the frequencies of two pairs are identical. The latter terms denote the interaction between emitter pairs, and $J_{\rm RS}$ is the effective four-body Rabi oscillation rate. Similarly to the discussion for the DBS, only the modes around $K_0 = \pm\pi/2$ are excited with high probabilities. Therefore, we can simplify $J_{\rm SR}$ as

$$J_{\rm RS} \simeq \frac{\mathcal{G}_{K_0}(n_1, n_2)\mathcal{G}^*_{K_0}(n_3, n_4)}{\sqrt{\delta_{II}\alpha}} \exp\left(-\frac{D_q}{L^B_{II}}\right), \tag{41}$$

which exponentially decreases as D_q, the same decay length as the DBS. In addition, emitters within the same pair are required to emit or absorb virtual photons concurrently, i.e., $\mathcal{G}_{iK} \neq 0$. Therefore, $d^e_{1,2}$ should be considerably smaller than the correlation length $\max\{L^-_c(K_0), L^B_I\}$. Eventually, we summarize the parameter regimes, where the four-body Rabi oscillations occur with a high fidelity:

$$\begin{aligned} &1.\quad d^e_{1,2} \leqslant \max\left\{L^-_c(K_0), L^B_I\right\}, \\ &2.\quad L^B_I < D_q \sim L^B_{II}. \end{aligned} \tag{42}$$

By considering the parameters in Fig. 3, the length scales can be computed as follows: $L^B_{II} \simeq 9$, $L^B_I \simeq 1.6$, and $L^-_c(K_0) \simeq 1.4$. When D_q and $d^e_{1,2}$ satisfy the conditions in Eq. (42), the four-body Rabi oscillation happens with a high fidelity, which amplitude is $A_{\rm RS} \simeq 1$, as shown in Fig. 5(a). Once $d^e_2 > 2$, i.e., $\mathcal{G}_{2K} = 0$, the second emitter pair decouple to the doublon mode, which cannot simultaneously absorb two virtual photons in the DBS. Consequently, the exchange process vanishes [see Fig. 5(b)]. Specifically, it is crucial to maintain a certain separation between the two pairs of emitters. When $D_q \approx L^B_I$, the undesired transitions mediated by the SPBSs will disrupt the four-body Rabi oscillations, and the single-photon transition amplitude A_μ cannot be neglected, which can be confirmed by the evolution in Fig. 5(c). In Figs. 6(a) and 6(b), we plot A_μ and $J_{\rm RS}$ versus D_q. When two emitter pairs are separated $D_q > 4$, the single-photon transitions are supersuppress, and the SPBSs are negligible $A_\mu \simeq 0$. Moreover, owing to the van Hove singularity at doublon band edges, the DBSs can distribute over a distance of tens of unit cells, and the four-body Rabi oscillation occurs when two emitter pairs are separated a long distance. Even when $D_q > 10$, $J_{\rm RS}$ is nonzero [see Fig. 6(b)].

When the coupling layout of second pair is changed, the four-body interaction vanishes. However, this four-body interaction has a special robustness against the frequency shift. In Fig. 6(c), we plot $A_{\rm RS}$ versus the frequency detuning of the second pair, i.e., $\delta_{3,4} = \omega_{3,4} - \omega_q$ by fixing the frequency of the first pair as $\omega_{q1,q2} = \omega_q$. Notably, when the summation frequency of the pair is fixed (i.e., $\delta_3 + \delta_4 = 0$), the detuning of each emitters hardly affects the four-body Rabi oscillation. For detunings $\{\delta_3, \delta_4\}$ far away from the anticorrealtion line $\delta_3 + \delta_4 = 0$, the oscillation amplitude $A_{\rm RS}$ quickly vanishes to zero. Those phenomena indicate that two photons are jointly

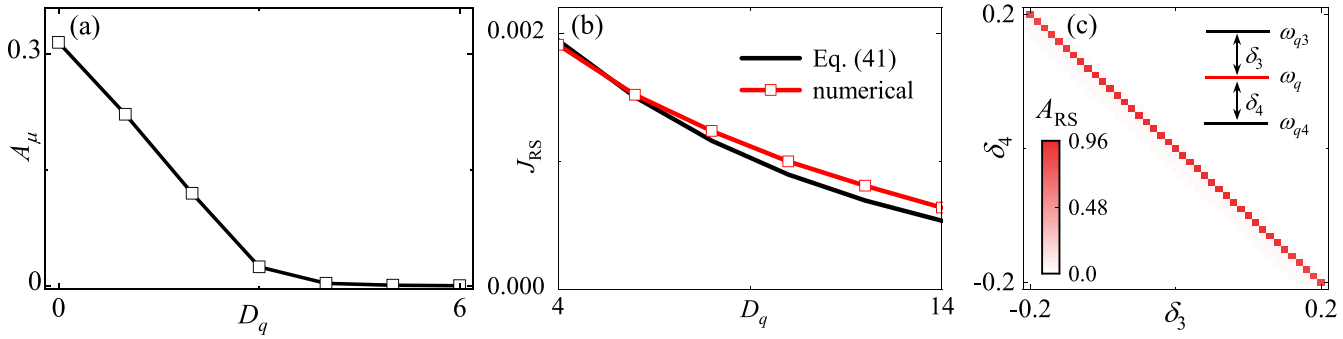

FIG. 6. (a) The single-photon transition amplitude A_μ versus D_q. (b) The four-body interaction strength J_{RS} versus D_q. The curve marked with symbols is obtained through numerical simulation, while the solid curve is plotted according to Eq. (41). (c) Amplitude of the four-body Rabi oscillation A_{RS} versus $\delta_{3,4}$. Same parameters as in Fig. 4(a).

emitted or absorbed and behave as a single quasiparticle. Therefore, we realize the four-body Rabi oscillations between two emitter pairs via the doublon bound state. With appropriate parameters, the fidelity of the oscillations can reach 100% and the distance between two pairs can reach tens of unit cells with still maintaining a high-fidelity. Therefore, our proposal exhibits the potential to realize multibody interactions between distant sites.

V. CONCLUSION

Here we have shown that both DBSs and SPBSs can be observed in a hybrid system of nonlinear waveguide and emitter pairs. By appropriately tuning the system parameters, we can control the relative amplitude, for contributing to the system dynamics, of DBS and SPBS. Moreover, a simplified form of the four-body interaction can only be realized via mediation of DBSs. We analyze the conditions for realizing high-fidelity four-body Rabi oscillations between two remote emitter pairs. Our proposal can be extended to a lattice chain with emitter pairs hopping together via the four-body interactions, which have potential applications in, for example, lattice-gauge theory simulations [80,81].

The coupled transmon array, which has been experimentally studied in quantum simulations [82–84], can be configured as a nonlinear waveguide in this study. The hopping strength J in circuit-QED can be engineering into strong coupling regime with $J \simeq 500$ MHz [85–87]. As indicated in Fig. 4, the four-body interaction strength can be around $J_{SR} \simeq 0.5 \sim 1$ MHz. In current circuit-QED experimental setups, the intrinsic dissipation rate of an individual transmon is around $\gamma/(2\pi) \simeq 5$ KHz [88,89], which is much weaker than J_{RS}. Additionally, theoretical study in Ref. [62] also showed the slow dissipation of the waveguide has little effect on the quantum phenomena with doublons. Therefore, we believe that the predicted four-body interaction is possible to observe in circuit-QED setups. Therefore, the observation of the predicted novel mechanisms is within current experimental reach. As an outlook, this study opens a new research direction in exploring exotic phenomena in nonlinear waveguide QED. In the future, it is intriguing to consider the coupling of emitter pairs to topological waveguides [90] and investigate its nonlinear chiral quantum optics [91].

ACKNOWLEDGMENTS

The quantum dynamical simulations are based on open source code QuTiP [92,93]. X.W. is supported by the National Natural Science Foundation of China (NSFC; Grant No. 12174303), and the Fundamental Research Funds for the Central Universities (Grant No. xzy012023053). T.L. acknowledges the support from National Natural Science Foundation of China (Grant No. 12274142), the Fundamental Research Funds for the Central Universities (Grant No. 2023ZYGXZR020), Introduced Innovative Team Project of Guangdong Pearl River Talents Program (Grant No. 2021ZT09Z109), and the Startup Grant of South China University of Technology (Grant No. 20210012). A.M. was supported by the Polish National Science Centre (NCN) under the Maestro Grant No. DEC-2019/34/A/ST2/00081. F.N. is supported in part by: Nippon Telegraph and Telephone Corporation (NTT) Research, the Japan Science and Technology Agency (JST) [via the CREST Quantum Frontiers program Grant No. JPMJCR24I2, the Quantum Leap Flagship Program (Q-LEAP), and the Moonshot R&D Grant Number JPMJMS2061], and the Office of Naval Research (ONR) Global (via Grant No. N62909-23-1-2074).

APPENDIX A: PROPERTIES OF THE BAND-EDGE MODES $K = \pm\pi/2$

In Fig. 2 of the main text, by considering a finite waveguide with periodic boundary conditions, we show the two-photon spectrum obtained by diagonalizing a nonlinear waveguide. Notably, we observe the emergence of a band gap within the doublon spectrum, and its width increases proportionally to the modulation strength U_m. The situation is similar to a conventional photonic crystal waveguide, where the eigen wave function at the band edge of is localized on sites possessing a low (high) refractive index. The distribution properties of the field are led by the destructive interference resulting from multiple reflections. Similarly, the behavior of doublons is also influenced by the periodic nonlinearity, and the characteristics of its wave function at the band edge resemble those of a single-photon crystal waveguide.

To substantiate the above discussions, we proceed to analyze the characteristics of the modes at $K_0 = \pi/2$. Concerning

the down/up energy levels, the eigenenergy is

$$E_{\mp} = -\sqrt{(U_c \pm U_m)^2 + 8J^2},$$

and the ratio in Eq. (24) is derived as

$$\frac{\psi_{K_0}^{(0)}(r=0)}{\psi_{K_0}^{(1)}(r=0)} = \frac{\frac{U_m}{U_c \pm U_m}}{1 - \frac{U_c}{U_c \pm U_m}} = \pm 1. \tag{A1}$$

Moreover, according to Eq. (21), the following relation is valid:

$$f_K^{(0)}(E_{\mp}, r) = f_K^{(1)}(E_{\mp}, r). \tag{A2}$$

For the down/up energy level at K_0, $f_K^{(0)}(E_{\mp}, r)$ derived as

$$\begin{aligned} f_K^{(0)}(E_{\mp}, r) &= \int \frac{e^{iqr}}{E_{\mp} + 4J\cos\left(\frac{K}{2}\right)\cos q} dq \\ &\propto \left(\frac{\sqrt{(U_c \pm U_m)^2 + 8J^2} - (U_c \pm U_m)}{2\sqrt{2}J} \right)^r \\ &= \exp\left[-\frac{r}{L_c^{\mp}(K_0)} \right], \end{aligned} \tag{A3}$$

where

$$\begin{aligned} \frac{1}{L_c^{\mp}(K_0)} &= \ln \frac{2\sqrt{2}J}{\sqrt{(U_c \pm U_m)^2 + 8J^2} - (U_c \pm U_m)} \\ &= \ln \frac{2\sqrt{2}J}{-E_{\mp} - \sqrt{E_{\mp}^2 - 8J^2}} \end{aligned}$$

is the decay length describing the joint probability of detecting two photons at the positions separated a distance r.

Equation (A3) implies that the doublon wave-function decays as the separation distance between two photons increases. By substituting Eqs. (A1)–(A3) into Eq. (25), one can find the wave functions at $K_0 = \pm\pi/2$ for the lower/upper energy levels

$$\begin{aligned} \Psi_{K_0}(x_c, r) &= \frac{1}{\sqrt{N}} e^{iK_0 x_c} \left[\psi_{K_0}^0(r) + e^{-i\pi x_c} \psi_{K_0}^1(r) \right] \\ &= \frac{1}{\sqrt{N}\psi_0} e^{iK_0 x_c} (1 \pm e^{-i\pi x_c}) \exp\left[-\frac{r}{L_c^{\mp}(K_0)} \right], \end{aligned} \tag{A4}$$

where ψ_0 is the normalized factor.

Now we summarize the characteristics of the doublon wave function around the band edge: First, due to the localized nature of the nonlinearity at each site, the maximum amplitude of $\Psi(E_{\mp}, x_c, r)$ occurs at $r = 0$ and rapidly diminishes as r increases [along the diagonal in Fig. 7(b)]. Second, the wave function exhibits periodic localization at sites with lower (higher) nonlinearity owing to the destructive interference of the multiple reflections. For the modes which are significantly distant from the band gap, the interference effect is weak due to the frequency and wave-vector mismatch, and the wave function distributes on both even and odd sites [see Fig. 7(b)].

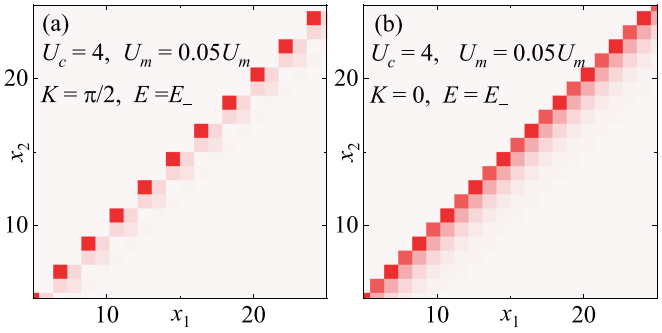

FIG. 7. Wave functions $\Psi(x_c, r)$ of the modes in the lower band at (a) $K = \pi/2$ and (b) $K = 0$, respectively. The waveguide parameters are the same as those in Fig. 2 in the main text.

APPENDIX B: DYNAMICS FOR EMITTER PAIRS INSIDE THE BAND GAP

1. Equations of motion

In this section, we derive the motion equation. By substituting Eqs. (28) and (29) into Schrödinger equation, we obtain the following coupled differential equations:

$$i\frac{dc_e(t)}{dt} = \frac{g}{\sqrt{N}} \sum_k [c_{1k}(t)e^{ikn_2} + c_{2k}(t)e^{ikn_1}], \tag{B1}$$

$$\begin{aligned} i\frac{dc_{1k}(t)}{dt} &= \delta_k c_{1k}(t) + \frac{g}{\sqrt{N}} c_e(t) e^{-ikn_2} \\ &\quad + g\sum_K M(K,k,n_1) c_K(t), \end{aligned} \tag{B2}$$

$$\begin{aligned} i\frac{dc_{2k}(t)}{dt} &= \delta_k c_{2k}(t) + \frac{g}{\sqrt{N}} c_e(t) e^{-ikn_1} \\ &\quad + g\sum_K M(K,k,n_2) c_K(t), \end{aligned} \tag{B3}$$

$$\begin{aligned} i\frac{dc_K(t)}{dt} &= \Delta_K c_K(t) + g\sum_k M^*(K,k,n_1) c_{1k}(t) \\ &\quad + g\sum_k M^*(K,k,n_2) c_{2k}(t), \end{aligned} \tag{B4}$$

$$\begin{aligned} M(K,k,n) &= \langle k,n|\Psi_K\rangle = \langle 0|\frac{1}{\sqrt{N}}\sum_m e^{-ikm} a_m a_n \\ &\quad \times \Psi_K(m',n') a_{m'}^\dagger a_{n'}^\dagger |0\rangle \\ &= \frac{\sqrt{2}}{N}\sum_m e^{-ikm} e^{iK(n+m)/2}\, u_K\left(\frac{m+n}{2}, n-m\right), \end{aligned} \tag{B5}$$

where $\delta_k = \omega_k - \omega_q$ with $\omega_k = -2J\cos k$ being the single-photon spectrum and $\Delta_K = E_K - 2\omega_q$. In our discussion, c_{ik} are the amplitudes of the single-photon intermediate states, which are extremely small due to the large detuning relation $\delta_k \gg g$. Consequently, one can adiabatically eliminate $c_{ik}(t)$ by assuming its evolution to be time independent. By setting $\dot{c}_{ik}(t) = 0$, Eqs. (B2) and (B3) result in

$$c_{jk}(t) = -\frac{g}{\delta_k}\left[\frac{e^{-ikn_j}}{\sqrt{N}} c_e(t) + \sum_K M(K,k,n_j) c_K(t) \right], \tag{B6}$$

where $j = 1, 2$. Altogether, by substituting Eq. (B6) into Eqs. (B1) and (B4), we end up with the coupled equations Eq. (30), in the main text.

In our work, we assume that the nonlinearity U_c is large and the doublon spectum is well separated from the scattering state. When the frequency of the emitter pair resides within the doublon band gap, both emitters are unable to completely release their energy into the nonlinear waveguide via supercorrelated emission channels. The probability $|c_e(t)|^2$ undergoes a phenomenon known as *fractional decay*. In other words, the excitation partially dissipates into the waveguide while also remaining localized within the two emitters.

Moreover, compared with the single-photon case, the field distribution on the waveguide is much more complex. First, because the single-emitter frequency ω_q lies outside of the single-photon band structure, i.e., $\omega_q < -2J$, there are SPBSs. Second, the coupled differential equations (30) and (31) indicate that a DBS containing two strong-correlated photons also exists in this system. In the following, we derive the field distributions for these two kinds of bound states.

2. Single-photon bound state

There are SPBSs originating from individual emitters. Their existences can be explicitly confirmed by analyzing Eq. (B6), which approaches a steady state in the long-time limit, leading to the generation of SPBSs. Considering the example of SPBS seeded by emitter 2, the steady-state population of the photonic component becomes

$$\begin{aligned}&\lim_{t\to\infty} c_{1k}(t)\\ &= -\lim_{t\to\infty}\frac{g}{\delta_k}\left[\frac{1}{\sqrt{N}}c_e(t)e^{-ikn_2}+\sum_K M(K,k,n_1)c_K(t)\right]\\ &\simeq -\lim_{t\to\infty}\frac{g}{\delta_k}\frac{1}{\sqrt{N}}e^{-ikn_2}c_e(t). \end{aligned}\tag{B7}$$

In our discussion, both the DBS and SPBS are only weakly excited. The excitations are mostly trapped inside the emitters, and we can approximate $c_K(t) \ll c_e(t) \simeq 1$. Therefore, the SPBS wave function is

$$\begin{aligned}\psi_2(n) &= \frac{1}{2\pi}\int_{-\pi}^{\pi}\frac{g}{w_e+2J\cos(k)}e^{ikn}e^{-ikn_2}dk\\ &\simeq \frac{g}{2\pi}\int_{-\pi}^{\pi}\frac{e^{ik(n-n_2)}}{w_e+2J\cos(k)}dk. \end{aligned}\tag{B8}$$

The SPBS produced by the emitter 1, i.e., $\psi_1(n)$, can also obtained by replacing $n_2 \to n_1$ in Eq. (B8). The SPBS for the emitter i can be written as

$$\psi_i(n) \simeq \frac{gJ}{\sqrt{(w_e)^2-4J^2}}\exp\left(-\frac{|n-n_i|}{L_I^B}\right),\tag{B9}$$

where the decay length L_I^B is

$$L_I^B = -\left(\ln\frac{-w_e-\sqrt{w_e^2-4J^2}}{2J}\right)^{-1}.\tag{B10}$$

In Fig. 8, we plot L_I^B as a function of the single emitter frequency ω_q, which shows that with increasing ω_q, the decay length of the SPBS decreases rapidly. At $\omega_q = -2.5J$, the decay length is approximately $L_I^B \simeq 1$. Therefore, when δ_I is large, the SPBS is strongly localized around the coupling point.

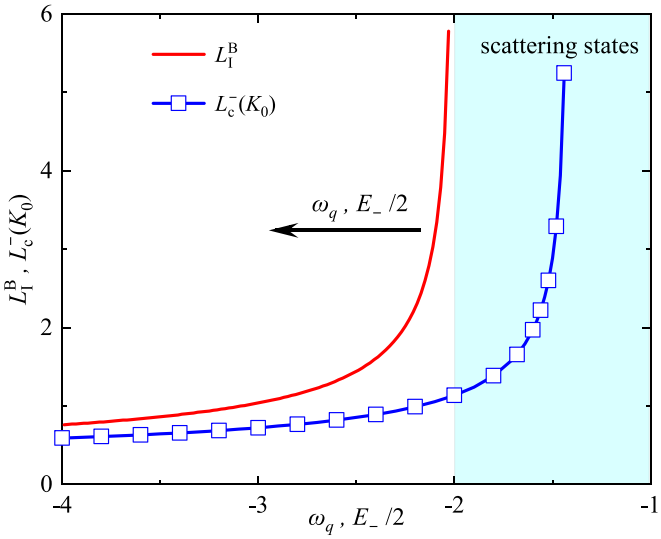

FIG. 8. Decay length L_I^B of the SPBS (the correlation length $L_c^-(K_0)$ for the DBS mode K_0), versus the emitter frequency ω_q (mode frequency $E_-/2$). The waveguide parameters are the same as those in Fig. 3 in the main text.

3. Doublon bound state

We derive the DBS wave function. Given that two emitters are initially excited, we rewrite the coupled differential Eqs. (30) and (31) in the Laplace space, i.e.,

$$s\tilde{c}_e(s) - 1 = i\frac{1}{\sqrt{N}}\sum_K \mathcal{G}_K(n_1,n_2)\tilde{c}_K(s),\tag{B11}$$

$$(s+i\Delta_K)\tilde{c}_K(s) = i\frac{1}{\sqrt{N}}\mathcal{G}_K^*(n_1,n_2)\tilde{c}_e(s).\tag{B12}$$

The above equations give

$$\begin{aligned}\tilde{c}_e(s) &= \frac{1}{s+\Sigma_e(s)},\\ \Sigma_e(s) &= \frac{1}{N}\sum_K |\mathcal{G}_K(n_1,n_2)|^2\frac{1}{(s+i\Delta_K)}, \end{aligned}\tag{B13}$$

where $\Sigma_e(s)$ can be interpreted as the self-energy. The real-time evolution is recovered as

$$c_e(t) = \frac{1}{2\pi i}\lim_{E\to\infty}\int_{\epsilon-iE}^{\epsilon+iE}\frac{1}{s+\Sigma_e(s)}e^{st}ds, \quad \epsilon > 0.\tag{B14}$$

Note that the emitter-pair frequency is quite close to the lower band edge of the doublon. Therefore, only the modes around $K_0 = \pi/2$ are excited with high probabilities.

Before moving forward, we conduct a numerical analysis of the properties of the coefficient $\mathcal{G}_K(n_i, n_j)$. As depicted in Fig. 9, where $1.75 < |\mathcal{G}_K(n_i,n_j)| < 1.95$ $(n_i = n_j = 0)$, we observe that $\mathcal{G}_K(n_i,n_j)$ varies within a narrow range versus K. Therefore, we can approximate it independent of K with $\mathcal{G}_K(n_1,n_2) \simeq \mathcal{G}_{K_0}(n_1,n_2)$. Moreover, we assume that the

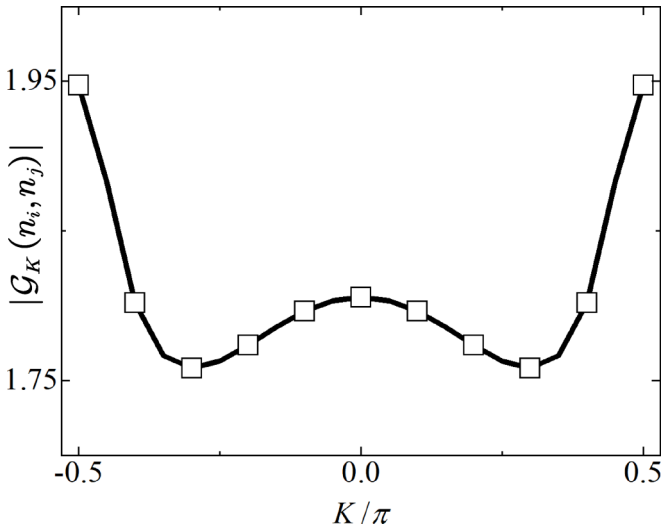

FIG. 9. Amplitude of the coefficient $\mathcal{G}_K(n_i, n_j)$ versus the wave vector K with $g = 1$. Here we set $n_i = n_j = 0$. The parameters are the same as those in Fig. 3 used in the main text.

dispersion relation around the edge of the lower band is described by a quadratic form, i.e., $\Delta_K \simeq \delta_{II} + \alpha(K - \pi/2)^2$ around $K = \pi/2$. By replacing the summation over K with an integral, the self energy can be written as

$$\Sigma_e(s) \simeq \frac{\left|\mathcal{G}_{K_0}(n_1, n_2)\right|^2}{\pi} \int_0^\pi dK \frac{1}{s + i[\delta_{II} + \alpha(K - \pi/2)^2]} \simeq \left|\mathcal{G}_{K_0}(n_1, n_2)\right|^2 \frac{1}{\sqrt{(is - \delta_{II})\alpha}}, \tag{B15}$$

where we have extended the integral bound to infinity. By substituting Eq. (B15) into Eq. (B14), we derive the steady-state population for $c_e(t)$ via the residue theorem, i.e.,

$$\lim_{t\to\infty} |c_e(t)|^2 = |\mathrm{Res}(s_0)|^2, \tag{B16}$$

where s_0 is the unique pure imaginary pole for the denominator of $\tilde{c}_e(s)$, i.e., $s_0 + \Sigma_e(s_0) = 0$, and

$$\mathrm{Res}(s_0) = \left.\frac{1}{1 + \partial_s \Sigma_e(s)}\right|_{s=s_0} = \frac{1}{1 - \frac{\alpha}{2}\left|\mathcal{G}_{K_0}(n_1, n_2)\right|^2 [(s_0 + i\delta_{II})\alpha]^{-\frac{3}{2}}}. \tag{B17}$$

By following the process of evaluating non-Markovian dynamics in Sec. II, one can also analysis non-Markovian to Markovian transition for this supercorrelated decay process. Now we derive the steady field distribution in the waveguide, i.e., the DBS. In the long-time limit $t \to \infty$, we set $\dot{c}_K(t) = 0$ in Eq. (31). The steady amplitude for mode K is

$$\lim_{t\to\infty} c_K(t) = \frac{1}{\sqrt{N}\Delta_K} \mathcal{G}_K^*(n_1, n_2)\mathrm{Res}(s_0). \tag{B18}$$

Be denoting $x_m = (n_1 + n_2)/2$ as the center position of the two emitters, the wave function of the DBS can be expressed as follows:

$$\begin{aligned}\Psi_d(x_c, r) &= \sum_K c_K(t_\infty) \frac{1}{\sqrt{N}\psi_0} e^{iKx_c} u_K(x_c, r) \\ &= \frac{\mathrm{Res}(s_0)}{\pi\psi_0} \int_0^\pi \mathcal{G}_K^*(n_1, n_2) u_K(x_c, r) \frac{e^{iK(x_c - x_m)}}{\Delta_K} dK \\ &\simeq \frac{\mathrm{Res}(s_0)}{\pi\psi_0} \mathcal{G}_{K_0}^*(n_1, n_2) u_{K_0}(x_c, r) \int_{-\infty}^\infty \frac{e^{i\delta K(x_c - x_m)}}{\delta_{II} + \alpha\delta K^2} d\delta K,\end{aligned} \tag{B19}$$

where we assume that $u_K(x_c, r)$ is also independent of K since only the modes around $K_0 = \pi/2$ are excited with high probabilities. Moreover, we approximate $\mathcal{G}_K(n_1, n_2) \simeq \mathcal{G}_{K_0}(n_1, n_2)$ as a constant in Eq. (B19). Finally, the wave function for the DBS is derived as

$$\Psi_d(x_c, r) = A_d \mathrm{Res}(s_0) u_{K_0}(x_c, r) e^{-\frac{|x_c - x_m|}{L_{II}^B}}, \quad A_d = \frac{\mathcal{G}_{K_0}^*(n_1, n_2)}{\psi_0\sqrt{\delta_{II}\alpha}}, \quad L_{II}^B = \sqrt{\frac{\alpha}{\delta_{II}}}. \tag{B20}$$

Given that the largest fraction of the energy is still trapped inside the emitters, we approximate $|\mathrm{Res}(s_0)| \simeq 1$ and Eq. (B20) is simplified as Eq. (36), in the main text.

APPENDIX C: FOUR-BODY INTERACTIONS BY EXCHANGING DOUBLONS

Let us now consider a scenario involving four emitters, forming two pairs that couple to the same waveguide (refer to Fig. 1 in the main text). We assume that the initial two excitations are localized within emitter 1 and 2, i.e., $c_{12}^e(t_0) = 1$, and the corresponding state is denoted as $|eegg\rangle$. In principle, the populations $c_{13}^e(t)$, $c_{23}^e(t)$, $c_{24}^e(t)$, and $c_{14}^e(t)$ are nonzero due to exchanging a single photon when the SPBSs in different pairs overlap. For instance, through the exchange of one photon between the emitters 1 and 3, the single-photon transition $|eegg\rangle \to |egeg\rangle$ occurs. To observe high-fidelity four-body Rabi oscillations between $c_{12}^e(t)$ and $c_{34}^e(t)$, it is crucial to suppress undesired single-photon processes. This can be achieved by positioning the emitter pairs at a distance significantly greater than the decay length of SPBS, i.e.,

$$D_q = (n_3 + n_4 - n_1 - n_2)/2 \gg L_I^B.$$

Under these conditions, the populations

$$c_{13}^e(t),\ c_{23}^e(t),\ c_{24}^e(t),\ c_{14}^e(t) \simeq 0,$$

and the system evolution is reduced to

$$i\dot{c}_{12}^e(t) = -\frac{1}{\sqrt{N}} \sum_K \mathcal{G}_{1K} c_K(t), \tag{C1}$$

$$i\dot{c}_{34}^e(t) = -\frac{1}{\sqrt{N}} \sum_K \mathcal{G}_{2K} c_K(t), \tag{C2}$$

$$i\dot{c}_K(t) = \Delta_{K_d} c_K(t) - \frac{1}{\sqrt{N}}\left[\mathcal{G}_{1K}^* c_{12}^e(t) + \mathcal{G}_{2K}^* c_{34}^e(t)\right], \tag{C3}$$

where

$$\mathcal{G}_{1K} = \mathcal{G}_K(n_1, n_2), \quad \mathcal{G}_{2K} = \mathcal{G}_K(n_3, n_4).$$

The doublon mode K can mediate the coherent exchange of excitations between the two emitters. In our analysis, the doublon is virtually excited, allowing us to adiabatically eliminate its degree of freedom by assuming $\dot{c}_K(t) = 0$. Finally, the coupled differential equations are reduced to

$$i\dot{c}^e_{12}(t) = -\frac{1}{N}\sum_K \frac{\left[|\mathcal{G}_{1K}|^2 c^e_{12}(t) + \mathcal{G}_{1K}\mathcal{G}^*_{2K} c^e_{34}(t)\right]}{\Delta_K}, \quad \text{(C4)}$$

$$i\dot{c}^e_{34}(t) = -\frac{1}{N}\sum_K \frac{\left[|\mathcal{G}_{2K}|^2 c^e_{34}(t) + \mathcal{G}_{2K}\mathcal{G}^*_{1K} c^e_{12}(t)\right]}{\Delta_K}. \quad \text{(C5)}$$

One can find that Eqs. (C4) and (C5) correspond to an effective Hamiltonian Eq. (38), in the main text.

[1] R. Mitsch, C. Sayrin, B. Albrecht, P. Schneeweiss, and A. Rauschenbeutel, Quantum state-controlled directional spontaneous emission of photons into a nanophotonic waveguide, Nat. Commun. **5**, 5713 (2014).

[2] P. Lodahl, S. Mahmoodian, and S. Stobbe, Interfacing single photons and single quantum dots with photonic nanostructures, Rev. Mod. Phys. **87**, 347 (2015).

[3] J. S. Douglas, H. Habibian, C. L. Hung, A. V. Gorshkov, H. J. Kimble, and D. E. Chang, Quantum many-body models with cold atoms coupled to photonic crystals, Nat. Photon. **9**, 326 (2015).

[4] K. Y. Bliokh and F. Nori, Transverse and longitudinal angular momenta of light, Phys. Rep. **592**, 1 (2015).

[5] T. Shi, Y.-H. Wu, A. González-Tudela, and J. I. Cirac, Bound states in boson impurity models, Phys. Rev. X **6**, 021027 (2016).

[6] P. Lodahl, S. Mahmoodian, S. Stobbe, A. Rauschenbeutel, P. Schneeweiss, J. Volz, H. Pichler, and P. Zoller, Chiral quantum optics, Nature (London) **541**, 473 (2017).

[7] A. González-Tudela and J. I. Cirac, Markovian and non-Markovian dynamics of quantum emitters coupled to two-dimensional structured reservoirs, Phys. Rev. A **96**, 043811 (2017).

[8] Y. B. Liu and A. A. Houck, Quantum electrodynamics near a photonic bandgap, Nat. Phys. **13**, 48 (2017).

[9] G. Trainiti and M. Ruzzene, Non-reciprocal elastic wave propagation in spatiotemporal periodic structures, New J. Phys. **18**, 083047 (2016).

[10] D. E. Chang, J. S. Douglas, A. González-Tudela, C.-L. Hung, and H. J. Kimble, Colloquium: Quantum matter built from nanoscopic lattices of atoms and photons, Rev. Mod. Phys. **90**, 031002 (2018).

[11] I. n. García-Elcano, A. González-Tudela, and J. Bravo-Abad, Tunable and robust long-range coherent interactions between quantum emitters mediated by Weyl bound states, Phys. Rev. Lett. **125**, 163602 (2020).

[12] J.-S. Tang, W. Nie, L. Tang, M.-Y. Chen, X. Su, Y.-Q. Lu, F. Nori, and K.-Y. Xia, Nonreciprocal single-photon band structure, Phys. Rev. Lett. **128**, 203602 (2022).

[13] X. Wang and H.-R. Li, Chiral quantum network with giant atoms, Quantum Sci. Technol. **7**, 035007 (2022).

[14] M. Stewart, J. Kwon, A. Lanuza, and D. Schneble, Dynamics of matter-wave quantum emitters in a structured vacuum, Phys. Rev. Res. **2**, 043307 (2020).

[15] D. De Bernardis, F. S. Piccioli, P. Rabl, and I. Carusotto, Chiral quantum optics in the bulk of photonic quantum Hall systems, PRX Quantum **4**, 030306 (2023).

[16] R. Karplus and M. Neuman, The scattering of light by light, Phys. Rev. **83**, 776 (1951).

[17] E. Iacopini and E. Zavattini, Experimental method to detect the vacuum birefringence induced by a magnetic field, Phys. Lett. B **85**, 151 (1979).

[18] M. O. Scully and M. S. Zubairy, *Quantum Optics* (Cambridge University Press, Cambridge, UK, 1997).

[19] C. Cohen-Tannoudji, J. Dupont-Roc, and G. Grynberg, *Atom–Photon Interactions* (Wiley, Weinheim, Germany, 1998).

[20] D. F. Walls and G. J. Milburn, *Quantum Optics* (Springer, Berlin, 2007).

[21] L. Zhou, Z. R. Gong, Y.-X. Liu, C. P. Sun, and F. Nori, Controllable scattering of a single photon inside a one-dimensional resonator waveguide, Phys. Rev. Lett. **101**, 100501 (2008).

[22] J.-Q. Liao, Z. R. Gong, L. Zhou, Y.-X. Liu, C. P. Sun, and F. Nori, Controlling the transport of single photons by tuning the frequency of either one or two cavities in an array of coupled cavities, Phys. Rev. A **81**, 042304 (2010).

[23] G. S. Agarwal, *Quantum Optics* (Cambridge University Press, Cambridge, UK, 2012).

[24] A. Imamoğlu, H. Schmidt, G. Woods, and M. Deutsch, Strongly interacting photons in a nonlinear cavity, Phys. Rev. Lett. **79**, 1467 (1997).

[25] J.-Q. Liao and C. K. Law, Correlated two-photon transport in a one-dimensional waveguide side-coupled to a nonlinear cavity, Phys. Rev. A **82**, 053836 (2010).

[26] T. Peyronel, O. Firstenberg, Q.-Y. Liang, S. Hofferberth, A. V. Gorshkov, T. Pohl, M. D. Lukin, and V. Vuletić, Quantum nonlinear optics with single photons enabled by strongly interacting atoms, Nature (London) **488**, 57 (2012).

[27] Y. O. Dudin, L. Li, F. Bariani, and A. Kuzmich, Observation of coherent many-body Rabi oscillations, Nat. Phys. **8**, 790 (2012).

[28] D. E. Chang, V. Vuletić, and M. D. Lukin, Quantum nonlinear optics—photon by photon, Nat. Photon. **8**, 685 (2014).

[29] K. E. Dorfman, F. Schlawin, and S. Mukamel, Nonlinear optical signals and spectroscopy with quantum light, Rev. Mod. Phys. **88**, 045008 (2016).

[30] D. Roy, C. M. Wilson, and O. Firstenberg, *Colloquium:* Strongly interacting photons in one-dimensional continuum, Rev. Mod. Phys. **89**, 021001 (2017).

[31] S. Kruk, A. Poddubny, D. Smirnova, L. Wang, A. Slobozhanyuk, A. Shorokhov, I. Kravchenko, B. Luther-Davies, and Y. Kivshar, Nonlinear light generation in topological nanostructures, Nat. Nanotech. **14**, 126 (2019).

[32] S. Mahmoodian, M. Čepulkovskis, S. Das, P. Lodahl, K. Hammerer, and A. S. Sørensen, Strongly correlated photon transport in waveguide quantum electrodynamics with weakly coupled emitters, Phys. Rev. Lett. **121**, 143601 (2018).

[33] Y. Ke, A. V. Poshakinskiy, C. Lee, Y. S. Kivshar, and A. N. Poddubny, Inelastic scattering of photon pairs in qubit arrays with subradiant states, Phys. Rev. Lett. **123**, 253601 (2019).

[34] A. V. Poshakinskiy and A. N. Poddubny, Dimerization of many-body subradiant states in waveguide quantum electrodynamics, Phys. Rev. Lett. **127**, 173601 (2021).

[35] Y. Marques, I. A. Shelykh, and I. V. Iorsh, Bound photonic pairs in 2D waveguide quantum electrodynamics, Phys. Rev. Lett. **127**, 273602 (2021).

[36] A. S. Sheremet, M. I. Petrov, I. V. Iorsh, A. V. Poshakinskiy, and A. N. Poddubny, Waveguide quantum electrodynamics: Collective radiance and photon-photon correlations, Rev. Mod. Phys. **95**, 015002 (2023).

[37] M. Napolitano, M. Koschorreck, B. Dubost, N. Behbood, R. J. Sewell, and M. W. Mitchell, Interaction-based quantum metrology showing scaling beyond the Heisenberg limit, Nature (London) **471**, 486 (2011).

[38] A. Reiserer, S. Ritter, and G. Rempe, Nondestructive detection of an optical photon, Science **342**, 1349 (2013).

[39] I. Shomroni, S. Rosenblum, Y. Lovsky, O. Bechler, G. Guendelman, and B. Dayan, All-optical routing of single photons by a one-atom switch controlled by a single photon, Science **345**, 903 (2014).

[40] Q. Bin, X.-Y. Lü, F. P. Laussy, F. Nori, and Y. Wu, *n*-phonon bundle emission via the stokes process, Phys. Rev. Lett. **124**, 053601 (2020).

[41] M. Cordier, M. Schemmer, P. Schneeweiss, J. Volz, and A. Rauschenbeutel, Tailoring photon statistics with an atom-based two-photon interferometer, Phys. Rev. Lett. **131**, 183601 (2023).

[42] M. Cramer, A. Flesch, I. P. McCulloch, U. Schollwöck, and J. Eisert, Exploring local quantum many-body relaxation by atoms in optical superlattices, Phys. Rev. Lett. **101**, 063001 (2008).

[43] R. Ma, B. Saxberg, C. Owens, N. Leung, Y. Lu, J. Simon, and D. I. Schuster, A dissipatively stabilized Mott insulator of photons, Nature (London) **566**, 51 (2019).

[44] A. Eckardt, Colloquium: Atomic quantum gases in periodically driven optical lattices, Rev. Mod. Phys. **89**, 011004 (2017).

[45] A. Rubio-Abadal, M. Ippoliti, S. Hollerith, D. Wei, J. Rui, S. L. Sondhi, V. Khemani, C. Gross, and I. Bloch, Floquet prethermalization in a bose-hubbard system, Phys. Rev. X **10**, 021044 (2020).

[46] P.-C. Kuo, N. Lambert, A. Miranowicz, H.-B. Chen, G.-Y. Chen, Y.-N. Chen, and F. Nori, Collectively induced exceptional points of quantum emitters coupled to nanoparticle surface plasmons, Phys. Rev. A **101**, 013814 (2020).

[47] Q. Zhu *et al.*, Observation of thermalization and information scrambling in a superconducting quantum processor, Phys. Rev. Lett. **128**, 160502 (2022).

[48] N. Gemelke, X. Zhang, C.-L. Hung, and C. Chin, In situ observation of incompressible Mott-insulating domains in ultracold atomic gases, Nature (London) **460**, 995 (2009).

[49] P. Macha, G. Oelsner, J.-M. Reiner, M. Marthaler, S. André, G. Schön, U. Hübner, H.-G. Meyer, E. Il'ichev, and A. V. Ustinov, Implementation of a quantum metamaterial using superconducting qubits, Nat. Commun. **5**, 5146 (2014).

[50] T. Weißl, B. Küng, E. Dumur, A. K. Feofanov, I. Matei, C. Naud, O. Buisson, F. W. J. Hekking, and W. Guichard, Kerr coefficients of plasma resonances in Josephson junction chains, Phys. Rev. B **92**, 104508 (2015).

[51] A. M. Kaufman, M. E. Tai, A. Lukin, M. Rispoli, R. Schittko, P. M. Preiss, and M. Greiner, Quantum thermalization through entanglement in an isolated many-body system, Science **353**, 794 (2016).

[52] Y. Salathé *et al.*, Digital quantum simulation of spin models with circuit quantum electrodynamics, Phys. Rev. X **5**, 021027 (2015).

[53] G. Reithmaier, M. Kaniber, F. Flassig, S. Lichtmannecker, K. Müller, A. Andrejew, J. Vučković, R. Gross, and J. J. Finley, On-chip generation, routing, and detection of resonance fluorescence, Nano Lett. **15**, 5208 (2015).

[54] P. Roushan *et al.*, Spectroscopic signatures of localization with interacting photons in superconducting qubits, Science **358**, 1175 (2017).

[55] Z. Yan *et al.*, Strongly correlated quantum walks with a 12-qubit superconducting processor, Science **364**, 753 (2019).

[56] C. W. Sandbo Chang, C. Sabín, P. Forn-Díaz, F. Quijandría, A. M. Vadiraj, I. Nsanzineza, G. Johansson, and C. M. Wilson, Observation of three-photon spontaneous parametric down-conversion in a superconducting parametric cavity, Phys. Rev. X **10**, 011011 (2020).

[57] I. Carusotto, A. A. Houck, A. J. Kollár, P. Roushan, D. I. Schuster, and J. Simon, Photonic materials in circuit quantum electrodynamics, Nat. Phys. **16**, 268 (2020).

[58] E. Kim, X. Zhang, V. S. Ferreira, J. Banker, J. K. Iverson, A. Sipahigil, M. Bello, A. González-Tudela, M. Mirhosseini, and O. Painter, Quantum electrodynamics in a topological waveguide, Phys. Rev. X **11**, 011015 (2021).

[59] M. Scigliuzzo, G. Calajò, F. Ciccarello, D. Perez Lozano, A. Bengtsson, P. Scarlino, A. Wallraff, D. Chang, P. Delsing, and S. Gasparinetti, Controlling atom-photon bound states in an array of Josephson-junction resonators, Phys. Rev. X **12**, 031036 (2022).

[60] L. Qiao and J. Gong, Coherent control of collective spontaneous emission through self-interference, Phys. Rev. Lett. **129**, 093602 (2022).

[61] X. Zhang, E. Kim, D. K. Mark, S. Choi, and O. Painter, A superconducting quantum simulator based on a photonic-bandgap metamaterial, Science **379**, 278 (2023).

[62] Z. Wang, T. Jaako, P. Kirton, and P. Rabl, Supercorrelated radiance in nonlinear photonic waveguides, Phys. Rev. Lett. **124**, 213601 (2020).

[63] J. Talukdar and D. Blume, Two emitters coupled to a bath with Kerr-like nonlinearity: Exponential decay, fractional populations, and Rabi oscillations, Phys. Rev. A **105**, 063501 (2022).

[64] J. Talukdar and D. Blume, Undamped Rabi oscillations due to polaron-emitter hybrid states in a nonlinear photonic waveguide coupled to emitters, Phys. Rev. A **106**, 013722 (2022).

[65] J. Talukdar and D. Blume, Photon-induced dropletlike bound states in a one-dimensional qubit array, Phys. Rev. A **108**, 023702 (2023).

[66] K. Winkler, G. Thalhammer, F. Lang, R. Grimm, J. H. Denschlag, A. J. Daley, A. Kantian, H. P. Büchler, and P. Zoller, Repulsively bound atom pairs in an optical lattice, Nature (London) **441**, 853 (2006).

[67] R. Piil and K. Mølmer, Tunneling couplings in discrete lattices, single-particle band structure, and eigenstates of interacting atom pairs, Phys. Rev. A **76**, 023607 (2007).

[68] Y.-M. Wang and J.-Q. Liang, Repulsive bound-atom pairs in an optical lattice with two-body interaction of nearest neighbors, Phys. Rev. A **81**, 045601 (2010).

[69] M. Di Liberto, A. Recati, I. Carusotto, and C. Menotti, Two-body physics in the Su-Schrieffer-Heeger model, Phys. Rev. A **94**, 062704 (2016).

[70] M. A. Gorlach and A. N. Poddubny, Topological edge states of bound photon pairs, Phys. Rev. A **95**, 053866 (2017).

[71] G. Calajó, F. Ciccarello, D. Chang, and P. Rabl, Atom-field dressed states in slow-light waveguide QED, Phys. Rev. A **93**, 033833 (2016).

[72] M. E. Tai, A. Lukin, M. Rispoli, R. Schittko, T. Menke, D. Borgnia, P. M. Preiss, F. Grusdt, A. M. Kaufman, and M. Greiner, Microscopy of the interacting Harper–Hofstadter model in the two-body limit, Nature (London) **546**, 519 (2017).

[73] M. Lyubarov and A. Poddubny, Edge states of photon pairs in cavity arrays with spatially modulated nonlinearity, Phys. Rev. A **100**, 053813 (2019).

[74] J.-D. Chen, H.-H. Tu, Y.-H. Wu, and Z.-F. Xu, Quantum phases of two-component bosons on the Harper-Hofstadter ladder, Phys. Rev. A **102**, 043322 (2020).

[75] S. Flannigan and A. J. Daley, Enhanced repulsively bound atom pairs in topological optical lattice ladders, Quantum Sci. Technol. **5**, 045017 (2020).

[76] A. A. Stepanenko and M. A. Gorlach, Interaction-induced topological states of photon pairs, Phys. Rev. A **102**, 013510 (2020).

[77] Y. Xing, X. Zhao, Z. Lü, S. Liu, S. Zhang, and H.-F. Wang, Observing two-particle Anderson localization in linear disordered photonic lattices, Opt. Express **29**, 40428 (2021).

[78] A. Berti and I. Carusotto, Topological two-particle dynamics in a periodically driven lattice model with on-site interactions, Phys. Rev. A **105**, 023329 (2022).

[79] A. A. Stepanenko, M. D. Lyubarov, and M. A. Gorlach, Higher-order topological phase of interacting photon pairs, Phys. Rev. Lett. **128**, 213903 (2022).

[80] D. Marcos, P. Rabl, E. Rico, and P. Zoller, Superconducting circuits for quantum simulation of dynamical gauge fields, Phys. Rev. Lett. **111**, 110504 (2013).

[81] G. K. Brennen, G. Pupillo, E. Rico, T. M. Stace, and D. Vodola, Loops and strings in a superconducting lattice gauge simulator, Phys. Rev. Lett. **117**, 240504 (2016).

[82] Y. Ye, Z.-Y. Ge, Y. Wu, S. Wang, M. Gong, Y.-R. Zhang, Q. Zhu, R. Yang, S. Li, F. Liang, J. Lin, Y. Xu, C. Guo, L. Sun, C. Cheng, N. Ma, Z. Y. Meng, H. Deng, H. Rong, C.-Y. Lu, C.-Z. Peng, H. Fan, X. Zhu, and J.-W. Pan, Propagation and localization of collective excitations on a 24-qubit superconducting processor, Phys. Rev. Lett. **123**, 050502 (2019).

[83] O. Mansikkamäki, S. Laine, A. Piltonen, and M. Silveri, Beyond hard-core bosons in transmon arrays, PRX Quantum **3**, 040314 (2022).

[84] Z.-C. Xiang, K. Huang, Y.-R. Zhang, T. Liu, Y.-H. Shi, C.-L. Deng, T. Liu, H. Li, G.-H. Liang, Z.-Y. Mei, H. Yu, G. Xue, Y. Tian, X. Song, Z.-B. Liu, K. Xu, D. Zheng, F. Nori, and H. Fan, Simulating Chern insulators on a superconducting quantum processor, Nat. Commun. **14**, 5433 (2023).

[85] S. J. Bosman, M. F. Gely, V. Singh, A. Bruno, D. Bothner, and G. A. Steele, Multi-mode ultra-strong coupling in circuit quantum electrodynamics, npj Quantum Inf. **3**, 46 (2017).

[86] A. F. Kockum, A. Miranowicz, S. De Liberato, S. Savasta, and F. Nori, Ultrastrong coupling between light and matter, Nat. Rev. Phys. **1**, 19 (2019).

[87] L. Ding, M. Hays, Y. Sung, B. Kannan, J. An, A. Di Paolo, A. H. Karamlou, T. M. Hazard, K. Azar, D. K. Kim, B. M. Niedzielski, A. Melville, M. E. Schwartz, J. L. Yoder, T. P. Orlando, S. Gustavsson, J. A. Grover, K. Serniak, and W. D. Oliver, High-fidelity, frequency-flexible two-qubit fluxonium gates with a transmon coupler, Phys. Rev. X **13**, 031035 (2023).

[88] S. Krinner, N. Lacroix, A. Remm, A. Di Paolo, E. Genois, C. Leroux, C. Hellings, S. Lazar, F. Swiadek, J. Herrmann, G. J. Norris, C. K. Andersen, M. Müller, A. Blais, C. Eichler, and A. Wallraff, Realizing repeated quantum error correction in a distance-three surface code, Nature (London) **605**, 669 (2022).

[89] A. P. M. Place, L. V. H. Rodgers, P. Mundada, B. M. Smitham, M. Fitzpatrick, Z. Leng, A. Premkumar, J. Bryon, A. Vrajitoarea, S. Sussman, G. Cheng, T. Madhavan, H. K. Babla, X. H. Le, Y. Gang, B. Jäck, A. Gyenis, N. Yao, R. J. Cava, N. P. de Leon, and A. A. Houck, New material platform for superconducting transmon qubits with coherence times exceeding 0.3 milliseconds, Nat. Commun. **12**, 1779 (2021).

[90] W. Z. Ling, X. Wang, Z. X. Liang, T. Liu, Z. Yang, and F. Nori, Unconversional bound states in nonlinear topological waveguide QED (unpublished).

[91] X. Wang, J.-Q. Li, Z.-H. Wang, A. F. Kockum, L. Du, T. Liu, and F. Nori, Nonlinear chiral quantum optics with giant emitter pairs, arXiv:2404.09829.

[92] J. R. Johansson, P. D. Nation, and F. Nori, Qutip: An open-source Python framework for the dynamics of open quantum systems, Comput. Phys. Commun. **183**, 1760 (2012).

[93] J. R. Johansson, P. D. Nation, and F. Nori, QuTiP 2: A Python framework for the dynamics of open quantum systems, Comput. Phys. Commun. **184**, 1234 (2013).